A Survey of Wireless Power Transfer and a Critical Comparison of Inductive and Capacitive Coupling for Small Gap Applications

Jiejian Dai, *Student Member, IEEE*, and Daniel C. Ludois, *Member, IEEE*

***Abstract*—Inductive power transfer (IPT) and capacitive power transfer (CPT) are the two most pervasive methods of wireless power transfer (WPT). IPT is the most common and is applicable to many power levels and gap distances. Conversely, CPT is only applicable for power transfer applications with inherently small gap distances due to constraints on the developed voltage. Despite limitations on gap distance, CPT has been shown to be viable in kilowatt power level applications. This paper provides a critical comparison of IPT and CPT for small gap applications, wherein the theoretical and empirical limitations of each approach are established. A survey of empirical WPT data across diverse applications in the last decade using IPT and CPT technology graphically compares the two approaches in power level, gap distance, operational frequency, and efficiency, among other aspects. The coupler volumetric power density constrained to small gap sizes is analytically established through theoretical physical limitations of IPT and CPT. Finally, guidelines for selecting IPT or CPT in small gap systems are presented.**

***Index Terms*—Capacitive power transfer (CPT), inductive power transfer (IPT), noncontact, wireless power transfer (WPT).**

NOMENCLATURE

$Q_{\rm gap}$	Gap reactive power [V · A].
$P_{\rm out}$	Output power [W].
C	Coupling capacitance [nF].
L	Coupling inductance [nH].
$U_C\, I_C$	Coupling capacitor voltage [V] and current [A].
$I_L U_L$	Coupling inductor current [A] and voltage [V].
$\varepsilon_0 \varepsilon_r$	Vacuum permittivity and relative permittivity [F/m].
$\mu_0 \mu_r$	Vacuum permeability and relative permeability [H/m].
$B_{\rm max}$	Maximum magnetic flux density in the core [T].
$E_{\rm max}$	Maximum electric field strength in the air gap [V/m].
$J_{\rm max}$	Maximum current density in conductor [A/m^2].
$A_{\rm C}$	Electric/magnetic field cross-sectional area [m^2].
d	Gap distance [m].

Manuscript received October 15, 2014; revised January 11, 2015; accepted March 10, 2015. Date of publication March 20, 2015; date of current version July 10, 2015. This work was funded in part by the USA Department of Energy's EERE Program under Award EE0006829, titled "Brushless and Permanent Magnet Free Wound Field Synchronous Motors for EV Traction." Recommended for publication by Associate Editor M. Sawan.

The authors are with the Department of Electrical and Computer Engineering, University of Wisconsin, Madison, WI 53706 USA, and also with the Wisconsin Electric Machines and Power Electronics Consortium, Madison, WI 53706 USA (e-mail: jdai7@wisc.edu; ludois@wisc.edu).

Color versions of one or more of the figures in this paper are available online at http://ieeexplore.ieee.org.

Digital Object Identifier 10.1109/TPEL.2015.2415253

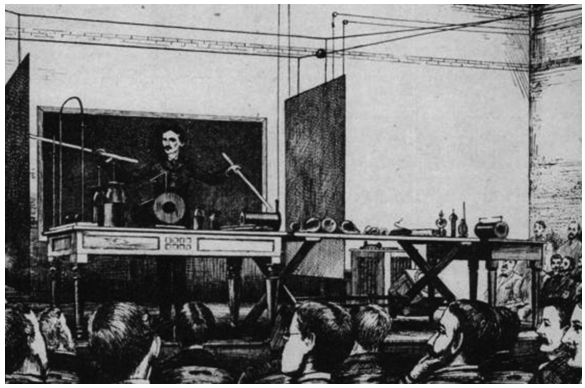

Fig. 1. Tesla demonstrating wireless power transmission using capacitive coupling at Columbia College, New York, in 1891.

$V_{\rm gap}$	Gap volume [m^3].
$V_{\rm coupler}$	Coupler volume [m^3].
r_g	Gap ratio ($d/\sqrt{A_C}$).
$r_A\, r_w$	Core dimension ratios (defined in Section III).
r_C	Capacitor coupler dimension ratio (defined in Section III).
k_C	Coupler volume coefficient.
k_w	Winding area fill factor.
$E_C\, D_C$	Coupling capacitor electric field in gap [V/m] [C/m^2].
$H_L\, B_L$	Coupling inductor magnetic field in gap [A/m] [T].
ρ_C	Coupling capacitor gap power density [W/m^3].
ρ_L	Coupling inductor gap power density [W/m^3].
$f_{\rm sw}$	Switching frequency [kHz].
f_0	Resonant frequency [kHz].
ω_0	Resonant angular velocity [rad/s].

I. INTRODUCTION

NEARLY all wireless power transfer (WPT) techniques use near-field electromagnetic induction, which can be divided into two methods: magnetic induction (or inductive power transfer—IPT) and electrostatic induction (or capacitive power transfer—CPT). The first public WPT demonstration to power a "commonplace" load was capacitive coupling to tube lighting by Tesla in 1891 [1], [2]. Fig. 1 illustrates the setting with Tesla and his tubes standing between the plates of a large capacitor. Electromagnetic induction over a distance was demonstrated shortly thereafter (again by Tesla) and proved to be more versatile for wireless power applications. Eventually, these techniques evolved into wireless communications. Continuing into the 1900s, Tesla's IPT methods progressed [3], [4] and some

far-field radiative techniques were also developed [5]. In the 1960s, use of IPT in biomedical applications kindled [6]–[9]. Higher power IPT research targeting electric highway systems started in the late 1970s [10], with some projects launched in the 1980s [11], but were unsuccessful due to the lack of good materials, semiconductor switches, and capacitors [12]. However, the lack of success highlighted the need for continued research and development in these areas. In the early to mid-1990s, IPT became established commercially in materials handling applications [12], roadway lighting [13], and the first commercial people mover (transport) systems were deployed [14]. As more consumer electronics chargers became mainstream from 1999 to 2012, IPT research and development renewed/pivoted again [15]–[18]. Development for dual functionality as a power transfer method and near-field communication (NFC) applications also occurred [19], [20]. Most recently, high-power IPT emerged as a means for electric vehicle charging [21]–[23]. However, until 2008, capacitive coupling for WPT remained largely overlooked since Tesla introduced it in 1891. From 2008 to 2014, CPT has experienced rapid development from several watt loads [24] to kilowatt-scale loads [25].

Although CPT is developing quickly, it is perceived as only suitable for low power levels over short transfer distances, while IPT is for low to high power levels spanning a larger distance range [26]. While CPT is limited in range to short gap distances, it is not necessarily limited in power level. To date, there has been no analytical or empirical research to establish the application boundaries between CPT and IPT, or give a guideline for what concept should be used in different applications of power level, gap distance, transmitter/receiver size, and cost. In this paper, a comprehensive survey of both IPT and CPT is given in Section II, illustrating the past, present, future, and application spaces of the two approaches. Section III provides a critical comparison between IPT and CPT coupling structures typical for small gap applications focused on power density for short transfer distances followed by discussion of guidelines for choosing the appropriate approach.

II. Survey of WPT Development

The aim of this section is to secure an understanding of the current capabilities of WPT as a whole, and how these capabilities have evolved over the last decade via a survey of published experimental work. Within this survey, the attributes of IPT and CPT will be examined empirically to establish trends and operational/application spaces for each technology.

A. Inductive Power Transfer

Table V in the appendix is a collection of recent major efforts to implement IPT technology, and these efforts are sorted by power transfer level from low to high. Very low power level (<1 W) applications tend to be biomedical implantable devices or sensors. These applications operate at a relatively high frequency, low efficiency, and a short gap distance. Low-power (1 W to <1 kW) applications typically are consumer electronics, e.g., cell phones, TVs, and lighting. Some niche biomedical applications may also get significant power but <1 kW. In this range, the efficiency, frequency, and gap distance vary greatly,

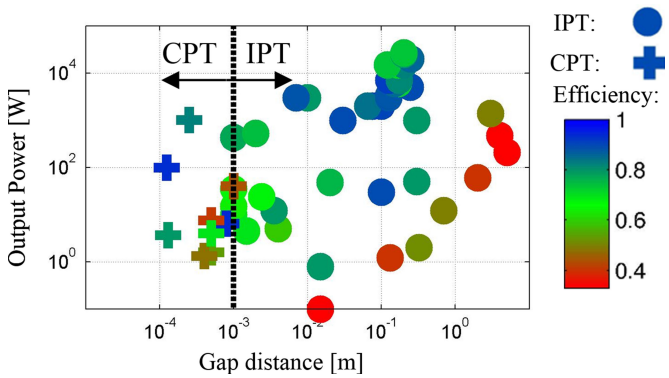

Fig. 2. Output power versus gap distance.

but short distance high-frequency IPT appears to have acceptable efficiency and cost as it is already commercialized. Longer distance low-power IPT systems are still in development. Deployed medium- to high-power level (>1 kW) applications include automotive assembly lines, clean factories, and general industrial automation applications. Research is ongoing into electric vehicle charging with interest growing steadily. These types of applications usually have a higher gap distance (e.g., >10 cm) and the operational frequency is generally low due to power electronics limitations.

B. Capacitive Power Transfer

Table VI in the appendix is a collection of recent major efforts to implement CPT technology, and these efforts are sorted by power transfer level as well. Compared with IPT, CPT is clearly still emerging as a viable option given the fewer points of reference, but the variety of applications is strikingly similar to IPT. CPT shares common applications with IPT, such as low-power biomedical devices and mobile device charging. Also, a clear trend of increasing power throughput is apparent with power levels approaching industrial automation and vehicle charging suitability. However, despite power level advancement, the physical limitations on air gaps generally preclude applications whose gap length is >1 mm.

C. Survey Data Analysis

The survey data assembled in the appendices is graphically compiled into Fig. 2–Fig. 7. These figures plot the empirical relationships between different aspects among IPT and CPT systems, namely power, efficiency, frequency, gap distance, coupler area, and volume. The plots establish general trends for IPT and CPT individually, as well as WPT as a whole over the last decade or so.

Fig. 2 plots power transfer capability versus transmitter to receiver gap distance with efficiency indicated by data point color. The figure clearly indicates that the IPT techniques are generally applicable in small to large gap regions (i.e., > 1 mm), while CPT techniques are applicable in very small to small gap regions (i.e., <1 mm). Although IPT is seen to have higher power capability based on surveyed research, it is evident that CPT power levels are increasing. Fig. 2 also indicates that both

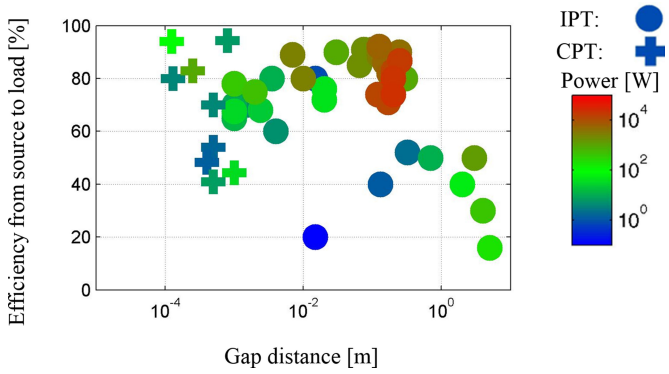

Fig. 3. Source to load efficiency versus gap distance.

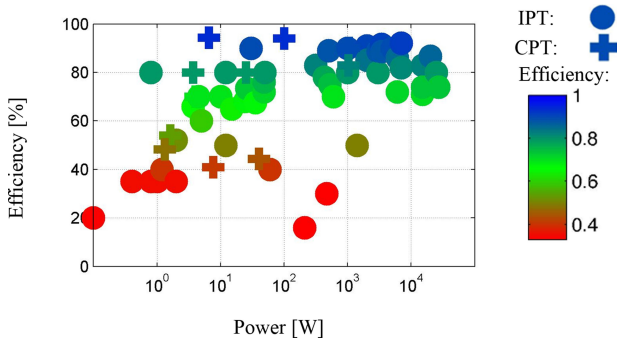

Fig. 4. Efficiency versus Power.

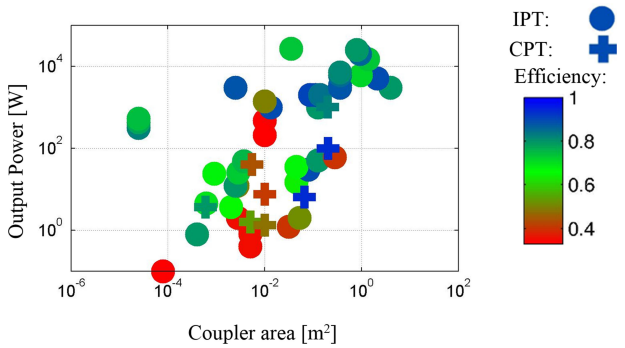

Fig. 5. Output power versus coupler area.

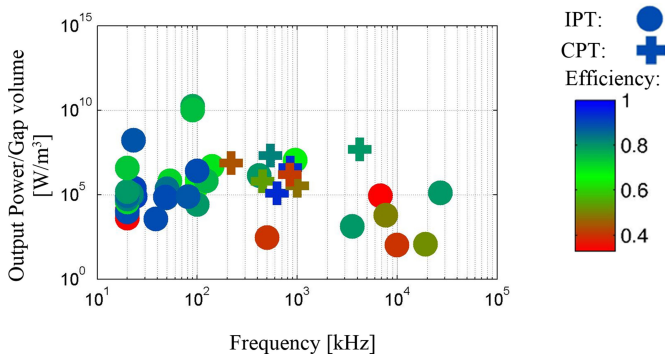

Fig. 6. Output power density $P_{\mathrm{out}}/V_{\mathrm{gap}}$ versus frequency.

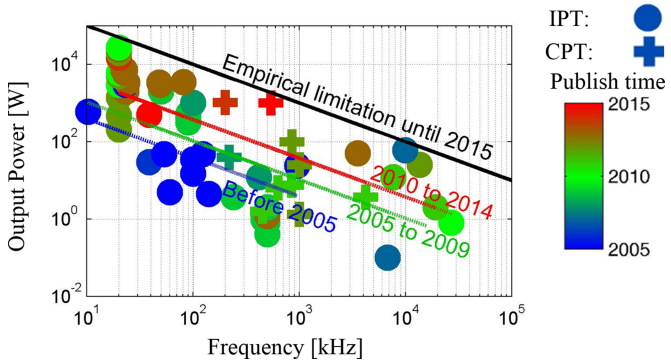

Fig. 7. Output power versus frequency with publication year.

IPT and CPT can achieve $\geq 90\%$ efficiency at kilowatt power levels in their respective gap ranges.

Fig. 3 plots source to load efficiency versus gap distance with data point power level indicated by color. This is the same data as contained within Fig. 2 but the axes have been reassigned. Again, it is clear that CPT is suitable for gaps <1 mm, and that IPT is suitable for larger gap distances. Interestingly, Fig. 3 suggests CPT possesses comparable or even greater efficiency than IPT for very small to small gap applications. As an overall trend for WPT, efficiency drops with increasing air gap but IPT is able to maintain $\sim$90% efficiencies for gaps up to tens of centimeter.

Fig. 4 plots the efficiency versus power level with color also indicating data point efficiency. Fig. 4 demonstrates that although IPT is able to transfer more power than CPT currently, CPT may have an efficiency advantage for applications of comparable power levels.

Fig. 5 plots the transmitter/receiver area versus throughput power with efficiency indicated by data point color. The coupler area is the cross-sectional area through which magnetic or electric fields transfer energy. In most cases, as shown in Tables V and VI, coupler area is defined as the receiver area. This is due to the form factor of some transmitters as elongated paths along which a mobile receiver can travel. Fig. 5 shows that as output power increases, larger coupling surfaces are needed. This is true for both IPT and CPT. At comparable power levels, the area needed for IPT and CPT is also comparable.

Fig. 6 plots gap power density versus operational frequency with data point efficiency indicated by color. The gap power density is calculated as the output power divided by the gap volume, and the gap volume is the gap distance multiplied by the coupler area.

Fig. 6 reveals that IPT can utilize a broad frequency range, 10's kHz to 10's MHz, while CPT utilizes a narrower higher frequency range, 100's kHz to 10's MHz. Within these respective frequency ranges, IPT and CPT are seen to achieve the same level of air gap power density. To be sure, the accuracy of this statement is subject to the previously identified constraints on IPT and CPT, namely that CPT is limited to small gaps.

Fig. 7 plots power transfer capability versus operational frequency with data point publication date indicated by color. Two trends may be observed from this plot. 1) As a whole, WPT (both IPT and CPT) throughput power decreases in a linear trend (for

TABLE I
WPT AVERAGE *Power–Frequency* PRODUCTS

Before 2005	$P_{\rm out} f_{\rm sw} = 10^{3.59}$ W · kHz
2005 to 2009	$P_{\rm out} f_{\rm sw} = 10^{4.02}$ W · kHz
2010 to 2014	$P_{\rm out} f_{\rm sw} = 10^{4.57}$ W · kHz
Best until 2015	$P_{\rm out} f_{\rm sw} = 10^{6}$ W · kHz

TABLE II
OBSERVATIONS ON SURVEYED IPT AND CPT DATA

	IPT	CPT
Frequency	10's kHz to 10's MHz	100's kHz to 10's MHz
Gap distance	10's cm (efficiently)	<1 mm
P–F product	$10\times$ increase in 10 years	
Power	∼Watt to ∼kilowatt with >90% efficiency possible	
Gap power density	Comparable air gap power density (power stored in overlapping operational spaces)	

a log scale) with frequency. It is likely that this limitation is primarily determined by power electronics limitations, rather than coupling characteristics, since it affects IPT and CPT equally. 2) The "*y*-intercept" of power versus frequency capability curves for distinct time periods of WPT is increasing. The current empirical limitation is plotted as a solid black line in Fig. 7 and is mathematically written as the power–frequency product (energy). The product specifically consists of output power $P_{\rm out}$ [W], and the operational frequency $f_{\rm sw}$ [kHz]. The output power is limited by losses as the frequency increases. This limitation appears in both IPT and CPT applications. The average power frequency product over four-year intervals starting at 2005 is summarized in Table I and graphically depicted in Fig. 7.

Between 2005 and 2014, the research community has advanced IPT and CPT of an order of magnitude in power–frequency capability. The average power increased $\sim 10\times$ in the last 10 years, and the frequency increased $\sim 10\times$ as well. This is attributable, in part, to the development of wide bandgap devices and refinement of coupling structures to minimize losses. It is expected that the power–frequency curve empirical limitation will continue to increase with time, essentially a "Moore's Law" trend or variant thereof for WPT.

D. General Survey Observations of IPT and CPT

After surveying the empirical data graphically, a number of generalized conclusions on IPT, CPT, and WPT as a whole are made in Table II.

Based on the conclusions above, IPT is broadly applicable; however, CPT is competitive with, and even potentially superior to, IPT for some small gap applications. This observation merits a deeper analytical inspection of the two coupling approaches with a strict focus on small gap applications where the operational spaces of IPT and CPT overlap. The following section provides a critical analytical comparison of the two techniques for small gaps (<1 mm) by examining the physics of common coupling structures used in these applications.

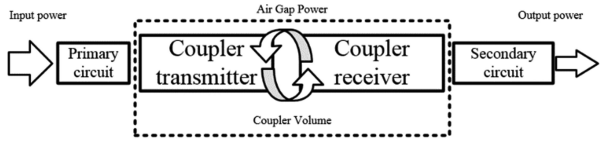

Fig. 8. Relationship between input/output power, gap power, and coupler volume.

III. IPT AND CPT ANALYTICAL COMPARISON FOR SMALL GAP APPLICATIONS

The previous section identified that either IPT or CPT may be used in small gap applications (<1 mm) with comparable air gap power density. This empirical comparison based on surveyed data provides high-level insight, but the finer details of the coupling structures themselves were not presented. This section critically compares IPT and CPT as they are commonly deployed for small gap applications, i.e., gapped permeable cores and parallel plate structures, respectively, by analytically examining field strength, coupler volume, and materials.

Power density is defined as the throughput power divided by the coupler volume (including the gap). To simplify the comparison between IPT and CPT, coupler power density is investigated rather than the overall system volume. The system combines the coupler, power electronics design, thermal management, and other mechanical design issues, which are beyond the scope of this paper. Fig. 8 illustrates the relationship between gap power, circuit power, and coupler size used for comparison.

To compare the power density, the gap energy density of the magnetic field and electric field is compared first (i.e., the electric/magnetic energy that can be stored in the gap volume). Then, the gap power density is used as an intermediate variable to establish a relationship between the air gap power and coupler volume. The IPT and CPT coupler geometries for analysis are illustrated in Fig. 9 with dimensional definitions assigned to calculate the volumes $V_{\rm gap}$ and $V_{\rm coupler}$.

Both IPT and CPT facing areas are defined as $A_{\rm C}$, separated by a gap of *d*, with both structures perfectly aligned. For small gap conditions, the IPT coupler herein is functionally a gapped transformer and modeled as two pot cores with identical center posts and back iron areas. The CPT couplers consist of two sets of parallel plates of identical surface area separated by a gap. It should be noted that for the CPT coupler, each of the square surfaces can be replaced by a stacked surface of *N* layers ($N = 3$ in Fig. 9(d2). As illustrated, the gap is divided into five pairs, and the surface thickness can be decreased to 1/3 as well. Although this is a different form factor, the total volume is unchanged.

The comparison may be more transparent if the couplers are redrawn from their actual implementation by lumping gaps and surface thicknesses together as in Fig. 9(b1) and (b2). Determining the volume of a CPT coupler is relatively straightforward. It is the sum of the gap volume and the volume of the coupling plates. IPT is less transparent; the core must be sized to accommodate space for windings, while simultaneously directing magnetic flux at a reasonable density in a closed path. For an IPT coupler, a spiral winding and pot core in Fig. 9(d1) is modeled in the same fashion as in Fig. 9(a1), just by increasing R_w and

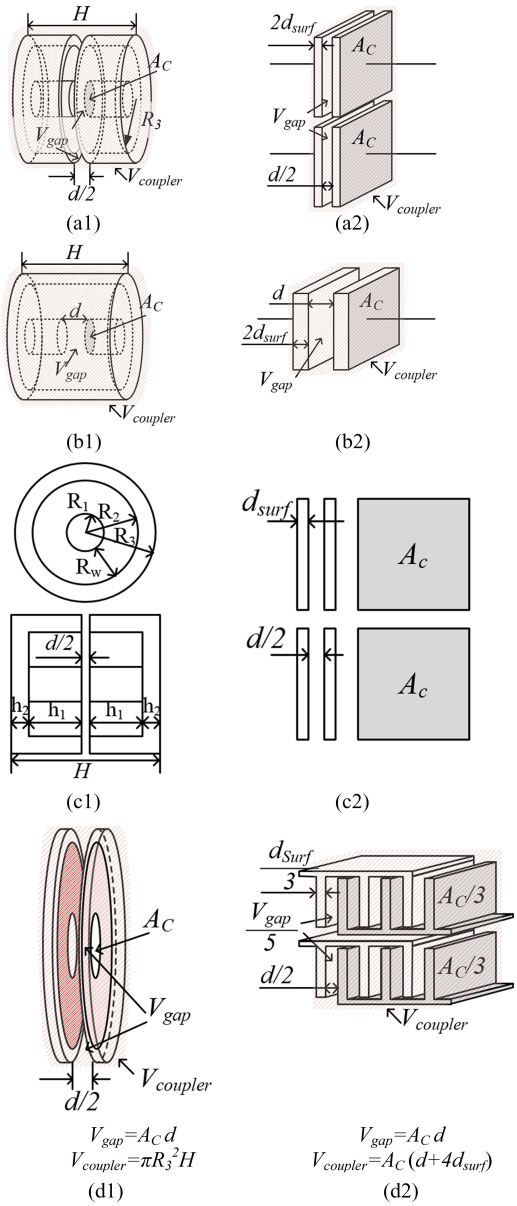

Fig. 9 Gap volume and coupler volume. (a1) IPT coupler. (a2) CPT coupler. (b1) IPT coupler equivalent. (b2) CPT coupler equivalent. (c1) IPT coupler dimensions. (c2) CPT coupler dimensions. (d1) IPT coupler example: Spiral winding . (d2) CPT coupler example: Stack array .

decreasing h_1. Ultimately, different dimensional permutations may be fed into these volume models suitable for analyzing coupler power density.

A. IPT Gap Energy Density

Field energy is stored in the gap. For the IPT system specified here, it is assumed that the current is purely sinusoidal with the peak value of I_L. The inductive reactive power and the power density are

$$Q_{\text{gap}} = \omega L I_{L\_\text{rms}}^2 = \pi f_{\text{sw}} \mu_0 \mu_r A_C d H_{L\_\max}^2 \tag{1}$$

$$\rho_L = \frac{Q_{\text{gap}}}{V_{\text{gap}}} = \pi f_{\text{sw}} \mu_0 \mu_r H_{L\_\max}^2 = \pi f_{\text{sw}} \frac{B_{L\_\max}^2}{\mu_0 \mu_r}. \tag{2}$$

In (2), the maximum magnetic field $H_{L\_\max}$ or induction $B_{L\_\max}$ is limited by the voltage integration over time (V/Hz), a familiar condition in inductive systems as described by

$$B_{L\_\max} = \mu_0 \mu_r H_{L\_\max} = \frac{1}{A_c} \frac{U_{L\_\max}}{2\pi f_{\text{sw}}}. \tag{3}$$

These formulae reveal the limiting factors concerning IPT throughput power. Namely, the power density is limited by the operational frequency and maximum flux density (energy stored in the gap). Operational frequency is determined by the loss characteristics of the power electronic drive circuitry and the coupler core (back iron) material. Additionally, the saturation properties of the core limit the peak value of flux density. Commonly used core materials such as ferrite or powdered iron regularly achieve flux densities of 0.2 T with core losses of 3 MW/m^3 and 10 MW/m^3, respectively, at a frequency of 500 kHz [27]. Depending on specific operating conditions, either saturation or core losses will determine the maximum flux density.

B. CPT Gap Energy Density

Similarly to IPT, the field energy is stored in the coupler gap. Unlike IPT, however, there is no core or back iron needed in a CPT system. Electric field lines terminate on charge and due to the cancellation of the field outside the coupling plates, a "back iron" pathway is not required. Thus, for a CPT system, the coupler volume will be only slightly larger (an integer multiple) than the gap itself. For the CPT system specified here, it is assumed that the voltage on the coupling capacitor is purely sinusoidal with a peak value of U_C. The capacitive reactive power and the power density are

$$Q_{\text{gap}} = \omega C U_{C\_\text{rms}}^2 = \pi f_{\text{sw}} \varepsilon_0 \varepsilon_r A_C d E_{C\_\max}^2 \tag{4}$$

$$\rho_C = \frac{Q_{\text{gap}}}{V_{\text{gap}}} = \pi f_{\text{sw}} \varepsilon_0 \varepsilon_r E_{C\_\max}^2 = \pi f_{\text{sw}} \frac{D_{C\_\max}^2}{\varepsilon_0 \varepsilon_r}. \tag{5}$$

Similar to (3), the displacement $D_{C\_\max}$ or electric field $E_{C\_\max}$ limits the current integration over time (A/Hz) as specified in (6) [28]. This reflects the physical duality between IPT and CPT: IPT—magnetic flux, CPT—electric charge

$$D_{C\_\max} = \varepsilon_0 \varepsilon_r E_{L\_\max} = \frac{1}{A_c} \frac{I_{C\_\max}}{2\pi f_{\text{sw}}}. \tag{6}$$

Much like IPT, CPT power density is limited by the operational frequency and gap displacement field strength. Without any core material or back iron as in IPT, the operational frequency is limited essentially by the power electronic drive circuitry because air gap losses are negligible. A limit on maximum field strength does exist, in the form of electric breakdown, rather than saturation [28], [29]. In air, the highest electric field possible under dry atmospheric conditions is ~3 kV/mm before breakdown occurs. This electric field strength is also indicative of why CPT is generally not utilized for applications with gap distances >1 mm, the resultant voltage between the transmitter and receiver plates is large. The field strength for CPT may be pushed higher in applications residing in vacuum or possibly when coatings are utilized to prevent a direct galvanic path between plates during gap (air) breakdown.

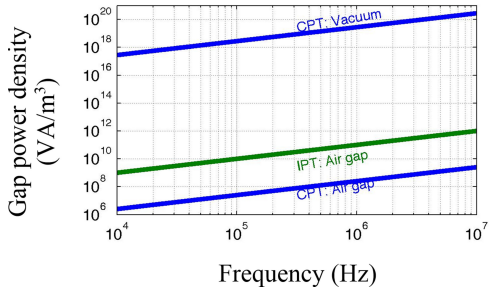

Fig. 10 IPT and CPT gap power density comparison ($B_{\max} = 0.2\ T, E_{\max} = 3\ \mathrm{MV/m}$).

TABLE III
WPT COUPLER GEOMETRY

	Name	Symbol	Expression (IPT)	Expression (CPT)
Common Parameters	Gap distance	d	d	
	Cross-sectional area	A_c	πR_1^2	A_c
	Gap geometry ratio	r_g	$\frac{d}{\sqrt{A_C}}$	
IPT Parameters	Winding area	A_w	$2h_1 R_w$	–
	Winding-core ratio	r_A	$\frac{A_w}{A_C}$	–
	Winding area geometry ratio	r_w	$\frac{R_w}{h_1}$	–
CPT Parameters	Surface thickness	d_{surf}	–	d_{surf}
	Thickness ratio	r_C	–	$\frac{d_{\mathrm{surf}}}{d}$

Fig. 10 plots the gap power density to compare IPT and CPT. The gap power density of the IPT system is substantially higher (∼400× larger) than CPT while operating in air. For further comparison, in vacuum the electric field strength may be *much* higher, allowing CPT to increase power density, while IPT is still limited by its core material. For a more complete picture of IPT and CPT power density, a thorough analysis of the coupler itself is needed. The gap volume is not the total volume; thus, the following section calculates and compares the volume of the couplers by including the core, windings, plate thickness, etc.

C. WPT Coupler Volume Calculations

Table III describes the pertinent variables for the IPT and CPT couplers in Fig. 9. For the sake of comparison, normalized ratios are used to describe the shape of the couplers.

1) IPT Coupler Size: According to Fig. 9(c1), the magnetic flux passes through three areas in the core, the center post πR_1^2, back iron $2\pi R_1 h_2$, and the core edge $\pi(R_3^2 - R_2^2)$. To prevent the flux density in the core from saturation, these three areas should be the same as defined in

$$A_C = \pi R_1^2 = 2\pi R_1 h_2 = \pi(R_3^2 - R_2^2). \tag{7}$$

Using the geometric definitions in Table III, the total IPT coupler volume V_{coupler} can be written as (8). Note that the factor k_C (˜1 : 1.1) is introduced to fulfill the extra volume that may be caused by the nonideal core shape (e.g., oversizing the core for winding area, saturation prevention area, etc.)

$$V_{\mathrm{coupler}} = \left[2h_1 + 2h_2 + \frac{d}{2}\right]\left[2A_C + \pi(R_2^2 - R_1^2)\right] k_C. \tag{8}$$

Next, V_{coupler} expressed in (8) may be normalized to the gap volume V_{gap} and after algebraic simplification, (9) is obtained

$$\frac{V_{\mathrm{coupler}}}{V_{\mathrm{gap}}} = \left[\frac{2}{r_g}\left(\sqrt{\frac{r_A}{2r_w}} + \sqrt{\frac{1}{4\pi}}\right) + \frac{1}{2}\right]\left[2 + \pi\left(\sqrt{\frac{2r_A r_W}{\pi}} + \frac{r_A r_W}{2}\right)\right] k_C. \tag{9}$$

Equation (9) indicates that the IPT coupler size is determined by three parameters: r_A, r_w, and r_g.r_A is determined by finding the winding area A_w of the IPT coupler (as in a transformer). To estimate A_w, (10) assumes that the current through each winding is the same with equal number of turns, while constraining the current density to be $J_{\max}$ with a fill factor of k_w. After substitution of (10) into Table III, the definition of r_A, r_A is written into terms of r_g and the gap volume V_{gap} in (11)

$$A_W = \frac{I_1 N_1 + I_1 N_1}{J_{\max} k_w} \approx \frac{2}{J_{\max} k_w}\frac{B_{\max} d}{\sqrt{2}\mu_0} \tag{10}$$

$$r_A \approx \frac{\sqrt{2}B_{\mathrm{sat}}}{J_{\max} k_w \mu_0}\frac{d}{A_C} = \frac{\sqrt{2}B_{\mathrm{sat}}}{J_{\max} k_w \mu_0}\frac{r_g^{\frac{4}{3}}}{V_{\mathrm{gap}}^{\frac{1}{3}}}. \tag{11}$$

Ultimately, (9) suggests that IPT possesses greater power density with lower r_A, which is intuitive because relative coupling area increases as r_A decreases. The empirical value for r_A should be around 0.5–2 [30]. However, the coupling area has an important impact on the parameter r_g, which is a significant factor affecting IPT coupler volume. With a small gap and large cross-sectional area (i.e., smaller r_g), the core may be easily saturated. Increasing the gap and decreasing the cross-sectional area will reduce this issue but the larger gap will cause the coupling factor to drop. Empirical values for r_g are typically 0.01–0.1 (e.g., For a 1-mm gap, the cross-sectional area is usually around 1–100 cm^2, and the gap volume is 0.1–10 cm^3) [31].

For every r_A and r_g, there is an optimal r_w to minimize V_{coupler} according to (9). Fig. 11 plots V_{coupler} normalized to V_{gap} (i.e., the coupler to gap volume ratio). As plotted in Fig. 11(a), the optimized r_w is generally between 0.1 and 1. For a spiral winding, the shape of the winding has larger area (R_w is high) and reduced depth (h_1 is small); therefore, $r_w (= R_w/h_1)$ is very high (e.g., > 10), increasing coupler volume to be larger than optimal, as shown in Fig. 11(b). For a general small gap, IPT coupler of the pot core design herein, the ratio $V_{\mathrm{coupler}}/V_{\mathrm{gap}}$ can be optimized to ∼100, and a typical value is ∼500. For example, a 1-mm gap (d), 10 cm × 10 cm cross-sectional area (A_C) coupler, at frequency 1 MHz, $V_{\mathrm{coupler}}/V_{\mathrm{gap}} = 498$.

2) CPT Coupler Size: Calculating V_{coupler} is easier for CPT since it has the advantage of being coreless. The only difference between gap volume and the coupler volume is the thickness of the conductive plate surfaces. The surface should be thick enough to carry current efficiently ($J_{\max} < 5$ A/mm^2). Also, its thickness should be manufactured practically (e.g., aluminum foil thickness $d_{\mathrm{A1}} = 0.025$ mm). The CPT coupler models are shown in Fig. 9(c2). Similar to the IPT coupler, a factor $k_C > 1$ is used to fulfill an operational safety or manufac-

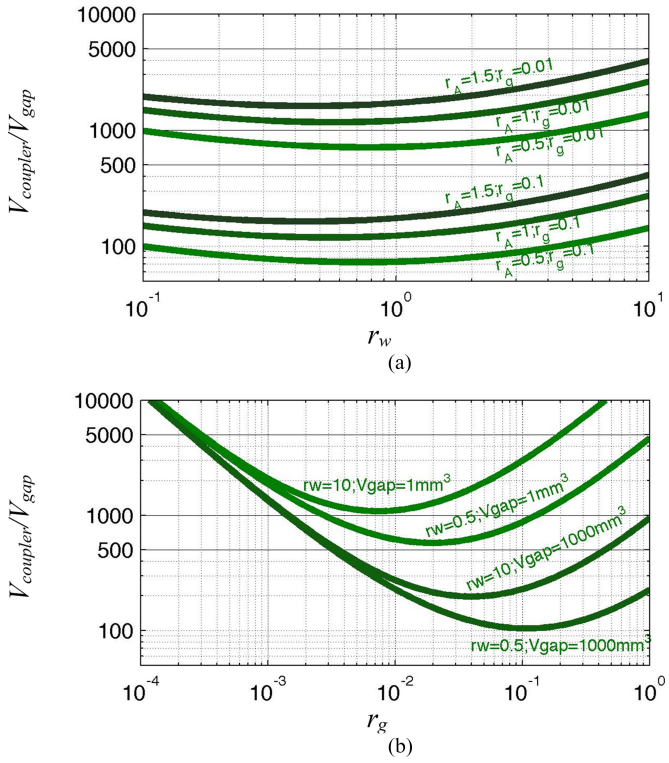

Fig. 11 Coupler volume optimization. (a) Optimization of r_w (with $r_A r_g$ fixed). (b) Coupler volume with different gap ratio r_g [with fixed r_w and optimized r_A in (11)] $B_{\rm sat} = 0.2\ T, k_w = 0.2, J_{\max} = 5\ {\rm A/mm}^2, k_C = 1$.

turability margin for extra coupling plate thickness should it be desired.

The surface thickness $d_{\rm surf\_e}$ for a square surface planar coupler may be sized using

$$I_C = J_{\max} d_{\rm surf\_e} \sqrt{A_C} = \frac{1}{\sqrt{2}} E_{\max} \omega \varepsilon A_C. \qquad (12)$$

After solving (12) for $d_{\rm surf\_e}$, and substitution into the ratios in Table III, the minimum surface thickness to satisfy electrical constraints is written as

$$d_{\rm surf\_e} = \frac{E_{\max}\omega\varepsilon\sqrt{A_C}}{\sqrt{2}J_{\max}} = \frac{E_{\max}\omega\varepsilon}{\sqrt{2}J_{\max}} \left(\frac{V_{\rm gap}}{r_g}\right)^{\frac{1}{3}}. \qquad (13)$$

Usually there are mechanical constraints as well, imposing a minimum thickness ($d_{\min}$) that can be manufactured. For off-the-shelf foils, the mechanical thickness is suitably large to satisfy electrical requirements. Assume $d_{\rm surf\_m} = d_{\min} = 0.025$ mm, which is the thickness of standard metal foils (~0.001 in). The thickness ratio in Table III is written as

$$r_C = \max\left(\frac{d_{\rm surf\_e}}{d}, \frac{d_{\rm surf\_m}}{d}\right) = \max\left(\frac{E_{\max}\omega\varepsilon}{\sqrt{2}J_{\max}}\frac{1}{r_g}, \frac{d_{\min}}{d}\right). \qquad (14)$$

The coupler to gap volume ratio is (15) after substitution of (14) into the coupler volume equation in Fig. 9

$$\frac{V_{\rm coupler}}{V_{\rm gap}} = (1 + 4r_C)\, k_C = \left[1 + \max\left(\frac{2\sqrt{2}E_{\max}\omega\varepsilon}{J_{\max} r_g}, \frac{4d_{\min}}{d}\right)\right] k_C. \qquad (15)$$

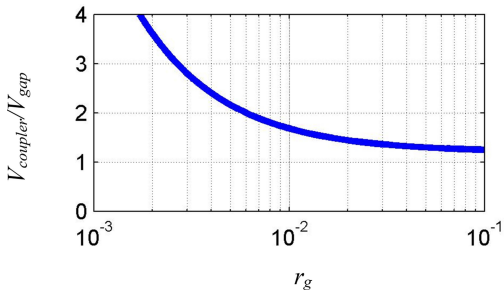

Fig. 12 Coupler/gap volume ratio versus gap/area ratio: Capacitive coupler volume optimization $E_{\max} = 3\ {\rm MV/m}, J_{\max} = 5\ {\rm A/mm}^2, f_{\rm sw} = 1\ {\rm MHz}, k_C = 1.2, A_C = 0.1\ {\rm m}^2$.

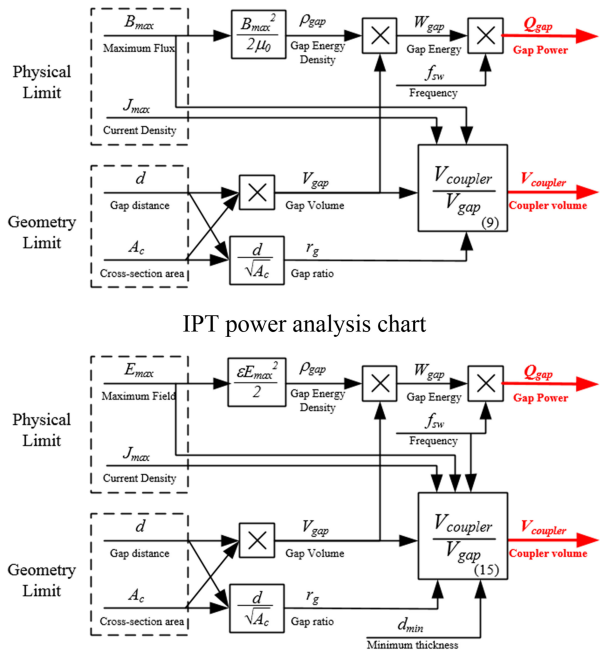

Fig. 13 Power density analysis chart. IPT power analysis chart. CPT power analysis chart.

As shown in Fig. 12, the volume ratio can be optimized to k_C (e.g., ~1.2), and the general value can be set to be (1–4) k_C. As an example, a 1-mm gap (d), 10 cm × 10 cm cross-sectional area (A_C) coupler, at frequency 1 MHz, if $k_C = 1.2$, $V_{\rm coupler}/V_{\rm gap} = 1.68$.

D. Discussion of Analytical Comparison of IPT and CPT Coupling and Correlation With Survey Data

Given the physical limitations of permeable material and air, along with volumetric constraints, an analysis of air gap power density and coupler volume for IPT and CPT was performed. Each coupling techniques' respective calculation process is documented in block diagram form in Fig. 13. Calculation blocks within the diagram refer back to the equations in the previous sections (equation numbers in lower right-hand corner of blocks). The coupler power density can be calculated by $Q_{\rm gap}/V_{\rm coupler}$. The air gap power $Q_{\rm gap}$ and the coupler volume $V_{\rm coupler}$ are limited by the material's physical characteristics

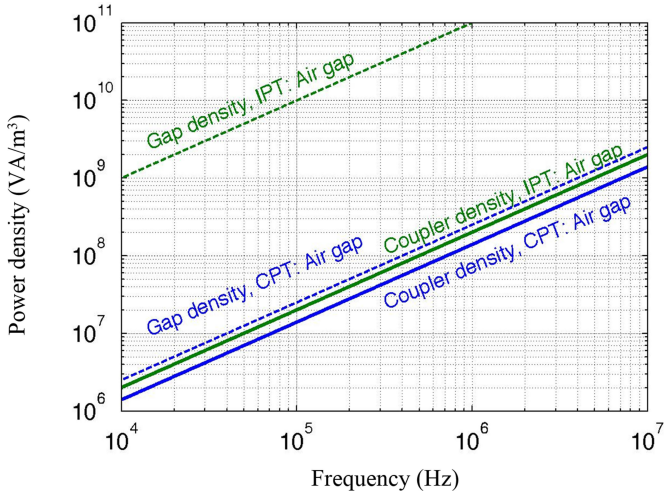

Fig. 14 Coupler power density and gap power density. When $d = 1$ mm, $Ac = 10\,\text{cm} \times 10\,\text{cm}$, capacitive coupler $V_{\text{coupler}}/V_{\text{gap}} \approx 1.68$, inductive coupler $V_{\text{coupler}}/V_{\text{gap}} \approx 500$.

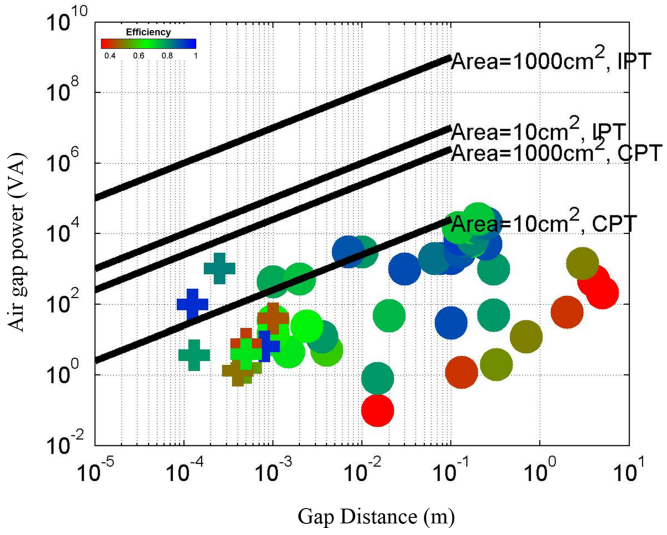

Fig. 15 Air gap power versus gap distance. Frequency: 1 MHz. Lines: Analytical data. Scatter points: Survey data.

(physical limits, i.e., saturation flux density, electric field strength, etc.) and the gap geometry requirements (geometry limits, i.e., gap distance d and transmitter/receiver area A_c).

In Sections III-A and III-B, it was calculated that IPT has ∼400× greater air gap energy storage capability than CPT under normal atmospheric conditions (air). Conversely, Section III-C demonstrated that the coupler to gap volume ratio favors CPT with a value of $V_{\text{coupler}}/V_{\text{gap}} = 1.68$ compared to the IPT best-case scenario of ∼100 and typical value of ∼500. This constitutes up to a ∼300× coupler to gap volume ratio advantage for CPT over IPT in small gap applications. The overall power density of these systems is reflected by the product of air gap power density and volume ratio as plotted in Fig. 14. Ultimately, Fig. 14 indicates that, despite disparate gap energy and coupler volumetric characteristics, IPT and CPT are roughly equivalent in power density for small gap applications. Another observation is that the coupler power density is much closer to the gap power density for the CPT technique.

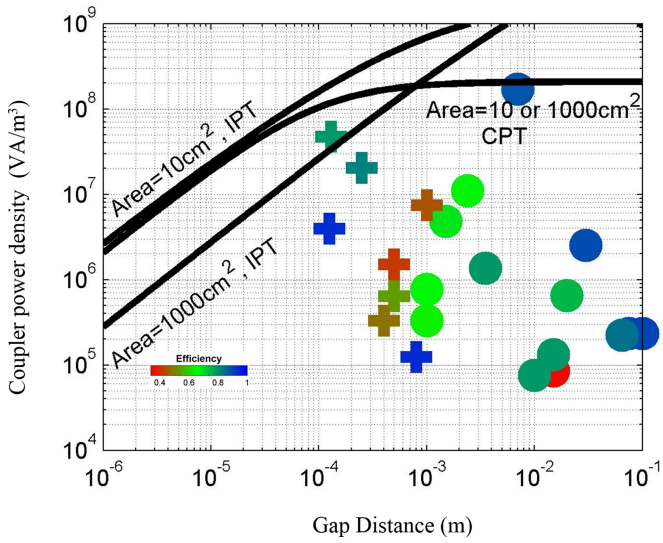

Fig. 16 Coupler power density versus air gap distance. Frequency: 1 MHz. Lines: Analytical data. Scatter points: Survey data.

TABLE IV
EMPIRICAL AND ANALYTICAL COMPARISON SUMMARY

Empirical Survey Results		
	IPT	CPT
Frequency	10's kHz ∼ 10's MHz	100's kHz ∼ 10's MHz
Gap distance	< 10's cm (efficiently)	< 1 mm
P–F product	10× increase in 10 years	
Power	∼Watt to ∼kilowatt with >90% efficiency possible	
Gap power density	Empirical data suggests comparable gap power density, Theoretical limit favors IPT	
Analytical Comparison of IPT and CPT		
	IPT	CPT
Power density is limited by	Core saturation flux (0.2 T) (Constant V/Hz)	Air gap electric field strength (3 MV/m) (Constant A/Hz)
Energy density	$\pi \frac{B^2_{L\_\max}}{\mu_0 \mu_r} = 10^5 \frac{J}{m^3}$	$\pi \varepsilon_0 \varepsilon_r E^2_{C\_\max} = 250 \frac{J}{m^3}$
$V_{coupler}/V_{\text{gap}}$	>100 ∼500	<4 ∼2
When does it have higher power?	Fixed gap distance	Fixed coupler volume
When does it have higher power density?	Gap $d > 1$ mm	Gap $d < 1$ mm
	Smaller transmitter/receiver area	

According to the analysis flow chart in Fig. 13, the following plots in Figs. 15 and 16 can be drawn to compare the suitable applications for IPT and CPT. In addition, theoretical limits are plotted against the surveyed data presented earlier in Section II. The analytical and surveyed data plotted together provide a level of verification of the analytical modeling. Limitation inputs for the model are $E_{\max} = 3\,\text{MV/m}$; $J_{\max} = 5\,\text{A/mm}^2$; $B_{\max} = 0.2$ T; $d_{\min} = 0.025$ mm; $k_w = 0.2$; and $f_{\text{sw}} = 1$ MHz.

Fig. 15 plots air gap power versus distance with efficiency indicated by color. In applications where the gap distance is fixed, and the coupler size is not a concern, IPT has the advantage of overall higher power capability. In applications where space is a commodity, CPT may have the advantage because of the lower coupler to gap volume ratio. Clearly, for a fixed gap, both

IPT and CPT exhibit the property that larger area allows higher coupler power as shown in Fig. 15.

Fig. 16 plots coupler power density verses gap distance with efficiency indicated by color. In applications where the coupler volume is fixed (rather than the gap), coupler power density $Q_{\mathrm{gap}}/V_{\mathrm{coupler}}$ is of greater concern. For small gaps ($<$1 mm), CPT has a higher power density. When the gap is $\sim$1 mm, CPT and IPT have similar power densities. For gaps >1 mm IPT has a better power density. This provides additional support to the notion that the boundary between IPT and CPT's efficacy with respect to gap size occurs at $\sim$1-mm gap, for a given coupling area.

IV. Conclusion

This paper surveyed the WPT landscape via empirical data and analytical modeling to compare IPT and CPT approaches. The empirical data revealed that WPT as a whole is capable of watt to kilowatt power levels with greater than 90% efficiencies in many cases. In the last decade, WPT has seen a tenfold increase in both power and operational frequency. The growth is expected to continue, given advances in wide bandgap semiconductors and coupler design approaches. In effect, a "Moore's Law" like trend is being established in the WPT community.

The surveyed data revealed an empirically established application boundary between IPT and CPT based on gap size. Overlap of IPT and CPT application spaces occurred at $\sim$1 mm, meriting a closer inspection in that gap range. An analytical comparison of applications with small air gaps ($\sim$1 mm or less) focused on IPT and CPT coupling structures that utilize gapped permeable cores and planar conductive surfaces, respectively. It should be noted that this inspection focused on inductive approaches rather than coupled resonator antennas, due to the small gap size. Given the magnetic core saturation flux and the electric field strength of the air, the IPT coupler air gap power density is potentially 400$\times$ greater than the CPT coupler under normal atmospheric conditions. However, because the magnetic flux needs a core ("back iron") to form a closed-loop path, the IPT coupler size is much larger than the gap size (>100$\times$, generally $\sim$500$\times$). In the case of the CPT coupler, the difference between coupler volume and gap volume is the thickness of the conductive surfaces, typically an integer multiple of the gap. The overall coupler volume can be made >4$\times$ the gap volume for CPT. As a result, the total power density of the IPT and CPT couplers are nearly the same for $\sim$1-mm gaps. Generally, gaps >1 mm favor IPT, and gaps $<$1 mm may favor CPT. General findings of the analytical comparison correlate with the empirical data. Table IV summarizes unique findings, both from the empirical data survey and theanalytical derivations.

Appendix

TABLE V
IPT Applications Deployment

Ref.	Power [W]	η[%]	Frequency [kHz]	Gap [mm]	Transmitter area [cm^2]	Receiver area [cm^2]	Institute	Year began
[32]	0.1	10 $\sim$ 20	6.78 MHz	15	21	0.785	University of Utah, UT	2007
[33]	0.4 $\sim$ 2	35	500		520	50	Philip, Germany	2009
[34]	0.794	80	27 MHz	15		$\sim$ 4	University of Newcastle, Australia	2010
[15], [35]	1		1 MHz	1.54	1	1	City U. Hongkong, Hong Kong	1999
[36]	1.2	40	500	130	314	314	KAIST, Korea	2013
[16]	1.3 $\sim$ 1.58		130		Hex pads	12	City U. Hongkong, Hong Kong	2005
[37]	3.7	66	240		288	20	University of Florida, FL	2009
[38]	4.5	60 $\sim$ 70	65 $\sim$ 140	1.5	6.24	6.24	Delta Electronics, Inc. NC	2003
[39]	5	60	$\sim$ 60	4			Kumamoto, Japan	2000
[17]	5		115 $\sim$ 200	2	$\sim$ 16	$\sim$ 16	Qi standard	2012
[40]	10	70	9.82	1			Tohoku Univ. Japan.	1996
[41]	12	50	7650	700	2734	2734	Intel Labs Seattle	2011
[42]	12	80	418	3.5	122	25	City U. Hongkong, Hong Kong	2008
[43]	15 $\sim$ 35	64.9 $\sim$ 67.6	100	1		$\sim$ 452	Tohoku Gakuin University, Japan	2002
[44]	24	68	950	2.4	9.08	9.08	Hanyang University, Korea	2004
[45]	25.6	73.4	13.56 MHz		$\sim$ 28.3	$\sim$ 28.3	Industrial Technology Research Institute, Taiwan	2012
[46]	30	90	38.4	100	792	792	University of Auckland, New Zealand	2006
[47], [48]	48	72 $\sim$ 76	53 $\sim$ 123	20	37	37	Virginia Polytechnic Institute & State University, VA	1992
[49]	50	80	3.54 MHz	300	1257	1257	Univ. of Wisconsin, Madison, WI	2013
[50]	60	60		500			Sony, Japan	2009
[51], [52]	60	40	9.9 MHz	2000	2827	2827	MIT, MA	2007

TABLE V
(CONTINUED)

Ref.	Power [W]	η[%]	Frequency [kHz]	Gap [mm]	Transmitter area [cm^2]	Receiver area [cm^2]	Institute	Year began
[53]	100		80				NCSU, NC	2011
[54]	100	97 coil	15.9 MHz	200	707	707	The University of Tokyo, Japan	2009
[55] $\sim$ [57]	10, 100, 209 $\sim$ 1403	16 $\sim$ 50, 95.4 coil	20	200, 3000 $\sim$ 7000	100 $\sim$ 1936	100 $\sim$ 1936	KAIST, Korea	2012
[58]	220	95 coil	3.7 MHz	300	908	908	Univ. of Wisconsin, Madison, WI	2011
[59]	315 $\sim$ 522	75 $\sim$ 83	90	0 $\sim$ 2	$\sim$ 0.25	$\sim$ 0.25	Instituto de Telecomunicações, Portugal	2009
[60]	390		10				Univ. of Auckland, New Zealand	2008
[61]	500	89	38.4				Univ. of Auckland, New Zealand	2010
[21], [62]	600		10.2				Univ. of Auckland, New Zealand	1994
[63], [64]	1 k	90	100	30 $\sim$ 300	133 $\sim$ 1257	133 $\sim$ 1257	Institut f. Automation u. Kommunikation, Germany	2004
[65]	1.5 k	95 coil	20	70	600	600	Saitama University, JAPAN	2010
[66], [67]	2 k	91	23.5	75	1134	855 $\sim$ 1134	ORNL, TN	2013
[68] $\sim$ [72]	2 k	85	5 $\sim$ 50	50 $\sim$ 80, 200	1385 $\sim$ 3849	1385 $\sim$ 3849	Univ. of Auckland, New Zealand	2009
[73]	3 k	89	22.95	6 $\sim$ 8	$\sim$ 25	$\sim$ 25	Grenoble Institute of Technology, France	1997
[74]	5 k	90	20	246	2.1 m^2	2.1 m^2	Utah State University, UT	2012
[23], [71], [75] $\sim$ [78]	2 $\sim$ 4 k; 6 $\sim$ 7 k	82 $\sim$ 92, 95 coil	22, 48 $\sim$ 81	125 $\sim$ 254	$\sim$ 3600	$\sim$ 3600	ORNL, TN	2011
[79]	7 k		20	125	3200	3200	Univ. of Auckland, New Zealand	2011
[14]	17 k		12.9	$\sim$ 50			Univ. of Auckland, New Zealand	2000
[22], [69], [80]–[83]	3 $\sim$ 25 k	71 $\sim$ 87	20	10 $\sim$ 250	(1 $\sim$ 14) $*$ N	990 $\sim$ 13 $*$ 103	KAIST, Korea	2010
[84] [85]	30 k		20	45	4800	4800	Univ. of Auckland, New Zealand	2005

TABLE VI
CPT APPLICATIONS DEPLOYMENT

Ref.	Power [W]	η[%]	Frequency [kHz]	Gap [mm]	Transmitter area [cm^2]	Receiver area [cm^2]	Note	Year began
[86]	0.0008		15 MHz	0.008	$8.1 * 10^{-5}$	$8.1 * 10^{-5}$	Johns Hopkins University, MD	2006
[87]	0.001 $\sim$ 0.1		250 $\sim$ 18000	0.1 $\sim$ 1	6.25	6.25	K. N. Toosi University of Technology, Iran	2009
[88]	1		1000	0.1	680	162	Univ. of Wisconsin, Madison, WI	2015
[89]	0 $\sim$ 1.46	0 $\sim$ 72	1000	0.4	750	100	Univ. of Auckland, New Zealand	2012
[90] [91]	1.6	54	449	0.5	50	50	Univ. of Auckland, New Zealand	2011
[92]	2		150	0.5			Univ. of Auckland, New Zealand	2009
[93]	3.7	80	4200	0.13	6	6	UC Berkeley, CA	2011
[94]	4	70		$\sim$ 0.5			Murata, Japan	2011
[95], [96]	6.5	94.3	626	0.8	817	653	Univ. of Wisconsin, Madison, WI	2011
[97]	7.6	41	840	0.5	100	100	Univ. of Auckland, New Zealand	2011
[98], [99]	10		20				Utunomiya University, Japan	2012
[100]	>25	>80	1000				Brunel University, UK	2012
[24]	40	44.3	217	1		$\sim$ 54	Univ. of Auckland, New Zealand	2008
[28]	100	94	848	0.125	2413	2011	Univ. of Wisconsin, Madison, WI	2014
[25]	1034	90.1	200				Univ. of Wisconsin, Madison, WI	2014
[101]	1021	83	540	0.25	2000	2000	Univ. of Wisconsin, Madison, WI	2015

ACKNOWLEDGMENT

The authors are grateful to the Wisconsin Electric Machines and Power Electronics Consortium for their continued support.

REFERENCES

[1] N. Tesla, *Experiments With Alternate Currents of Very High Frequency and Their Application to Methods of Artificial Illumination*. Radford, VA, USA: Wilder, 2008.

[2] T. C. Martin and N. Tesla, *The Inventions, Researches and Writings of Nikola Tesla, With Special Reference to His Work in Polyphase Currents and High Potential Lighting*. New York, NY, USA: The Electrical Engineer, 1894.

[3] H. W. Secor, "Tesla apparatus and experiments—How to build both large and small Tesla and Oudin coils and how to carry on spectacular experiments with them," *Pract. Electr.*, vol. 1, Nov. 1921.

[4] R. Lomas. (2014, Aug. 16). The man who invented the twentieth century. CERN Document Server. [Online]. Available: http://cds.cern.ch/record/404189

[5] N. Tesla, "System of transmission of electrical energy," U.S. Patent US 645 576, Mar 20, 1900.

[6] F. C. Flack, E. D. James, and D. M. Schlapp, "Mutual inductance of air-cored coils: Effect on design of radio-frequency coupled implants," *Med. Biol. Eng.*, vol. 9, no. 2, pp. 79–85, Mar. 1971.

[7] J. C. Schuder, J. H. Gold, and H. E. Stephenson, "An inductively coupled RF system for the transmission of 1 kW of power through the skin," *IEEE Trans. Biomed. Eng.*, vol. BME-18, no. 4, pp. 265–273, Jul. 1971.

[8] W. H. Ko, S. P. Liang, and C. D. F. Fung, "Design of radio-frequency powered coils for implant instruments," *Med. Biol. Eng. Comput.*, vol. 15, no. 6, pp. 634–640, Nov. 1977.

[9] N. de N. Donaldson and T. A. Perkins, "Analysis of resonant coupled coils in the design of radio frequency transcutaneous links," *Med. Biol. Eng. Comput.*, vol. 21, no. 5, pp. 612–627, Sep. 1983.

[10] J. G. Bolger, F. A. Kirsten, and L. S. Ng, "Inductive power coupling for an electric highway system," in *Proc. IEEE 28th Veh. Technol. Conf.*, 1978, vol. 28, pp. 137–144.

[11] I. Systems Control Technology, Roadway Powered Electric Vehicle Project Track Construction and Testing Program Phase 3D. California PATH Program, Institute of Transportation Studies, University of California, Berkeley, CA, USA, 1994.

[12] G. A. Covic and J. T. Boys, "Inductive power transfer," *Proc. IEEE*, vol. 101, no. 6, pp. 1276–1289, Jun. 2013.

[13] J. T. Boys and A. W. Green. (2015, Jan. 3). Intelligent road-studs—Lighting the paths of the future. [Online]. Available: http://search.informit.com.au/documentSummary;dn=911935860467184;res=IELENG

[14] G. A. Covic, G. Elliott, O. H. Stielau, R. M. Green, and J. T. Boys, "The design of a contact-less energy transfer system for a people mover system," in *Proc. Int. Conf. Power Syst. Technol.*, 2000, vol. 1, pp. 79–84.

[15] S. Y. R. Hui, H. S.-H. Chung, and S. C. Tang, "Coreless printed circuit board (PCB) transformers for power MOSFET/IGBT gate drive circuits," *IEEE Trans. Power Electron.*, vol. 14, no. 3, pp. 422–430, May 1999.

[16] S. Y. R. Hui and W. W. C. Ho, "A new generation of universal contactless battery charging platform for portable consumer electronic equipment," *IEEE Trans. Power Electron.*, vol. 20, no. 3, pp. 620–627, May 2005.

[17] Wireless Power Consortium, Qi System Description: Wireless Power Transfer, 1st ed., vol. I: Low Power, (2012). [Online]. Available: http://www.wirelesspowerconsortium.com/downloads/wireless-power-specification-part-1.html

[18] S. Y. R. Hui, W. Zhong, and C. K. Lee, "A critical review of recent progress in mid-range wireless power transfer," *IEEE Trans. Power Electron.*, vol. 29, no. 9, pp. 4500–4511, Sep. 2014.

[19] W.-S. Lee, K.-S. Oh, and J.-W. Yu, "Distance-Insensitive wireless power transfer and near-field communication using a current-controlled loop with a loaded capacitance," *IEEE Trans. Antennas Propag.*, vol. 62, no. 2, pp. 936–940, Feb. 2014.

[20] W.-S. Lee, W.-I. Son, K.-S. Oh, and J.-W. Yu, "Contactless energy transfer systems using antiparallel resonant loops," *IEEE Trans. Ind. Electron.*, vol. 60, no. 1, pp. 350–359, Jan. 2013.

[21] J. T. Boys, G. A. Covic, and A. W. Green, "Stability and control of inductively coupled power transfer systems," *IEE Proc. Electr. Power Appl.*, vol. 147, no. 1, pp. 37–43, Jan. 2000.

[22] J. Huh, S. W. Lee, W. Y. Lee, G. H. Cho, and C. T. Rim, "Narrow-Width inductive power transfer system for online electrical vehicles," *IEEE Trans. Power Electron.*, vol. 26, no. 12, pp. 3666–3679, Dec. 2011.

[23] P. Ning, J. M. Miller, O. C. Onar, and C. P. White, "A compact wireless charging system for electric vehicles," in *Proc. IEEE Energy Convers. Cong. Exp.*, 2013, pp. 3629–3634.

[24] A. Hu, C. Liu, and H. L. Li, "A novel contactless battery charging system for soccer playing robot," in *Proc. 15th Int. Conf. Mechatron. Mach. Vis. Practice*, 2008, pp. 646–650.

[25] J. Dai and D. Ludois, "Single active switch power electronics for kilowatt scale capacitive power transfer," *IEEE J. Emerg. Sel. Topics Power Electron.*, vol. 3, no. 1, pp. 315–323, Mar. 2015.

[26] F. Musavi and W. Eberle, "Overview of wireless power transfer technologies for electric vehicle battery charging," *IET Power Electron.*, vol. 7, no. 1, pp. 60–66, Jan. 2014.

[27] R-material datasheet. (Aug., 2014). [Online]. Available: http://www.mag-inc.com/products/ferrite-cores/r-material

[28] D. C. Ludois, M. J. Erickson, and J. K. Reed, "Aerodynamic fluid bearings for translational and rotating capacitors in noncontact capacitive power transfer systems," *IEEE Trans. Ind. Appl.*, vol. 50, no. 2, pp. 1025–1033, Mar./Apr. 2014.

[29] B. Ge, D. C. Ludois, and R. Perez, "The use of dielectric coatings in capacitive power transfer systems," in *Proc. IEEE Energy Convers. Congr. Expo.*, 2014, pp. 2193–2199.

[30] R. W. Erickson, *Fundamentals of Power Electronics*, 2nd ed. New York, NY, USA: Kluwer, 2004.

[31] C. W. T. McLyman, *Transformer and Inductor Design Handbook*, 3rd ed. New York, NY, USA: Marcel Dekker, 2004.

[32] R. R. Harrison, "Designing efficient inductive power links for implantable devices," in *Proc. IEEE Int. Symp. Circuits Syst.*, 2007, pp. 2080–2083.

[33] E. Waffenschmidt and T. Staring, "Limitation of inductive power transfer for consumer applications," in *Proc. 13th Eur. Conf. Power Electron. Appl.*, 2009, pp. 1–10.

[34] A. Laskovski and M. R. Yuce, "Class-E oscillators as wireless power transmitters for biomedical implants," in *Proc. 3rd Int. Symp. Appl. Sci. Biomed. Commun. Technol.*, 2010, pp. 1–5.

[35] S. Y. Hui, S. C. Tang, and H. S.-H. Chung, "Optimal operation of coreless PCB transformer-isolated gate drive circuits with wide switching frequency range," *IEEE Trans. Power Electron.*, vol. 14, no. 3, pp. 506–514, May 1999.

[36] E. Lee, X. Thai, S. Choi, C. Rim, and J. Huh, "Impedance transformers for compact and robust coupled magnetic resonance systems," in *Proc. IEEE Energy Convers. Congr. Expo.*, 2013, pp. 2239–2244.

[37] J. J. Casanova, Z. N. Low, and J. Lin, "Design and optimization of a Class-E amplifier for a loosely coupled planar wireless power system," *IEEE Trans. Circuits Syst. II Exp. Briefs*, vol. 56, no. 11, pp. 830–834, Nov. 2009.

[38] Y. Jang and M. M. Jovanovic, "A contactless electrical energy transmission system for portable-telephone battery chargers," *IEEE Trans. Ind. Electron.*, vol. 50, no. 3, pp. 520–527, Jun. 2003.

[39] H. Abe, H. Sakamoto, and K. Harada, "A noncontact charger using a resonant converter with parallel capacitor of the secondary coil," *IEEE Trans. Ind. Appl.*, vol. 36, no. 2, pp. 444–451, Mar. 2000.

[40] J. Murakami, F. Sato, T. Watanabe, H. Matsuki, S. Kikuchi, K. Harakawa, and T. Satoh, "Consideration on cordless power station-contactless power transmission system," *IEEE Trans. Magn.*, vol. 32, no. 5, pp. 5037–5039, Sep. 1996.

[41] A. P. Sample, D. A. Meyer, and J. R. Smith, "Analysis, experimental results, and range adaptation of magnetically coupled resonators for wireless power transfer," *IEEE Trans. Ind. Electron.*, vol. 58, no. 2, pp. 544–554, Feb. 2011.

[42] X. Liu and S. Y. R. Hui, "Optimal design of a hybrid winding structure for planar contactless battery charging platform," *IEEE Trans. Power Electron.*, vol. 23, no. 1, pp. 455–463, Jan. 2008.

[43] K. Hatanaka, F. Sato, H. Matsuki, S. Kikuchi, J. Murakami, M. Kawase, and T. Satoh, "Power transmission of a desk with a cord-free power supply," *IEEE Trans. Magn.*, vol. 38, no. 5, pp. 3329–3331, Sep. 2002.

[44] B. Choi, J. Nho, H. Cha, T. Ahn, and B. Choi, "Design and implementation of low-profile contactless battery charger using planar printed circuit board windings as energy transfer device," *IEEE Trans. Ind. Electron.*, vol. 51, no. 1, pp. 140–147, Feb. 2004.

[45] W. Chen, R. A. Chinga, S. Yoshida, J. Lin, C. Chen, and W. Lo, "A 25.6 W 13.56 MHz wireless power transfer system with a 94% efficiency GaN Class-E power amplifier," in *Proc. IEEE MTT-S Int. Microw. Symp. Dig.*, 2012, pp. 1–3.

[46] G. Covic, J. T. Boys, and H. G. Lu, "A three-phase inductively coupled power transfer system," in *Proc. 1st IEEE Conf. Ind. Electron. Appl.*, 2006, pp. 1–6.

[47] A. Ghahary and B. H. Cho, "Design of transcutaneous energy transmission system using a series resonant converter," *IEEE Trans. Power Electron.*, vol. 7, no. 2, pp. 261–269, Apr. 1992.

[48] G. B. Joun and B.-H. Cho, "An energy transmission system for an artificial heart using leakage inductance compensation of transcutaneous transformer," *IEEE Trans. Power Electron.*, vol. 13, no. 6, pp. 1013–1022, Nov. 1998.

[49] R. J. Calder, S.-H. Lee, and R. D. Lorenz, "Efficient, MHz frequency, resonant converter for sub-meter (30 cm) distance wireless power transfer," in *Proc. IEEE Energy Convers. Congr. Expo.*, 2013, pp. 1917–1924.

[50] (2014, Aug. 21). Sony. Sony-sony develops highly efficient wireless power transfer system. [Online]. Available: http://www.sony.net/SonyInfo/News/Press/200910/09–119E/

[51] A. Kurs, A. Karalis, R. Moffatt, J. D. Joannopoulos, P. Fisher, and M. Soljačić, "Wireless power transfer via strongly coupled magnetic resonances," *Science*, vol. 317, no. 5834, pp. 83–86, Jul. 2007.

[52] A. Karalis, J. D. Joannopoulos, and M. Soljacic, "Efficient wireless non-radiative mid-range energy transfer," *Ann. Phys.*, vol. 323, no. 1, pp. 34–48, Jan. 2008.

[53] Z. Pantic, S. Bai, and S. Lukic, "A new tri-state-boost-based pickup topology for inductive power transfer," in *Proc. IEEE Energy Convers. Congr. Expo.*, 2011, pp. 3495–3502.

[54] T. Imura, H. Okabe, and Y. Hori, "Basic experimental study on helical antennas of wireless power transfer for electric vehicles by using magnetic resonant couplings," in *Proc. IEEE Vehicle Power Propulsion Conf.*, 2009, pp. 936–940.

[55] B. H. Choi, E. S. Lee, J. H. Kim, and C. T. Rim, "7 m-off-long-distance extremely loosely coupled inductive power transfer systems using dipole coils," in *Proc. IEEE Energy Convers. Congr. Expo.*, 2014, pp. 858–563.

[56] C. Park, S.-W. Lee, and C.-T. Rim, "5m-off-long-distance inductive power transfer system using optimum shaped dipole coils," in *Proc. 7th Int. Power Electronics Motion Control Conf.*, 2012, vol. 2, pp. 1137–1142.

[57] H. Kim, C. Song, J. Kim, J. Kim, and J. Kim, "Shielded coil structure suppressing leakage magnetic field from 100 W-class wireless power transfer system with higher efficiency," in *Proc. IEEE Int. Microw. Workshop Series Innovative Wireless Power Transmiss., Technol., Syst. Appl.*, 2012, pp. 83–86.

[58] S.-H. Lee and R. D. Lorenz, "Development and validation of model for 95%-efficiency 220-W wireless power transfer over a 30-cm Air Gap," *IEEE Trans. Ind. Appl.*, vol. 47, no. 6, pp. 2495–2504, Nov. 2011.

[59] S. Valtchev, B. Borges, K. Brandisky, and J. B. Klaassens, "Resonant contactless energy transfer with improved efficiency," *IEEE Trans. Power Electron.*, vol. 24, no. 3, pp. 685–699, Mar. 2009.

[60] G. Covic, J. T. Boys, A. M. W. Tam, and J. C.-H. Peng, "Self tuning pick-ups for inductive power transfer," in *Proc. IEEE Power Electron. Spec. Conf.*, 2008, pp. 3489–3494.

[61] H. H. Wu, J. T. Boys, and G. Covic, "An AC processing pickup for IPT systems," *IEEE Trans. Power Electron.*, vol. 25, no. 5, pp. 1275–1284, May 2010.

[62] A. W. Green and J. T. Boys, "10 kHz inductively coupled power transfer-concept and control," in *Proc. 5th Int. Conf. Power Electron. Variable-Speed Drives*, 1994, pp. 694–699.

[63] R. Mecke and C. Rathge, "High frequency resonant inverter for contactless energy transmission over large air gap," in *Proc. IEEE 35th Annu. Power Electron. Spec. Conf.*, 2004, vol. 3, pp. 1737–1743.

[64] D. Kurschner and C. Rathge, "Contactless energy transmission systems with improved coil positioning flexibility for high power applications," in *Proc. IEEE Power Electron. Spec. Conf.*, 2008, pp. 4326–4332.

[65] Y. Nagatsuka, N. Ehara, Y. Kaneko, S. Abe, and T. Yasuda, "Compact contactless power transfer system for electric vehicles," in *Proc. Int. Power Electron. Conf.*, 2010, pp. 807–813.

[66] P. Ning, O. Onar, and J. Miller, "Genetic algorithm based coil system optimization for wireless power charging of electric vehicles," in *Proc. IEEE Transp. Electrification Conf. Expo.*, 2013, pp. 1–5.

[67] O. C. Onar, J. M. Miller, S. L. Campbell, C. Coomer, C. P. White, and L. E. Seiber, "A novel wireless power transfer for in-motion EV/PHEV charging," in *Proc. IEEE 28th Annu. Appl. Power Electron. Conf. Expo.*, 2013, pp. 3073–3080.

[68] M. Budhia, G. Covic, and J. T. Boys, "Design and optimization of circular magnetic structures for lumped inductive power transfer systems," *IEEE Trans. Power Electron.*, vol. 26, no. 11, pp. 3096–3108, Nov. 2011.

[69] A. Khaligh and S. Dusmez, "Comprehensive topological analysis of conductive and inductive charging solutions for plug-in electric vehicles," *IEEE Trans. Veh. Technol.*, vol. 61, no. 8, pp. 3475–3489, Oct. 2012.

[70] C.-Y. Huang, J. T. Boys, G. Covic, and M. Budhia, "Practical considerations for designing IPT system for EV battery charging," in *Proc. IEEE Vehicle Power Propulsion Conf.*, 2009, pp. 402–407.

[71] H. H. Wu, A. Gilchrist, K. Sealy, P. Israelsen, and J. Muhs, "A review on inductive charging for electric vehicles," in *Proc. IEEE Int. Electric Mach. Drives Conf.*, 2011, pp. 143–147.

[72] M. Budhia, G. Covic, and J. T. Boys, "Design and optimisation of magnetic structures for lumped inductive power transfer systems," in *Proc. IEEE Energy Convers. Congr. Expo.*, 2009, pp. 2081–2088.

[73] R. Laouamer, M. Brunello, J. Ferrieux, O. Normand, and N. Buchheit, "A multi-resonant converter for non-contact charging with electromagnetic coupling," in *Proc. 23rd Int. Conf. Ind. Electron., Control Instrum.*, 1997, vol. 2, pp. 792–797.

[74] H. H. Wu, A. Gilchrist, K. D. Sealy, and D. Bronson, "A high efficiency 5 kW inductive charger for EVs using dual side control," *IEEE Trans. Ind. Informat.*, vol. 8, no. 3, pp. 585–595, Aug. 2012.

[75] M. S. Chinthavali, O. C. Onar, J. M. Miller, and L. Tang, "Single-phase active boost rectifier with power factor correction for wireless power transfer applications," in *Proc. IEEE Energy Convers. Congr. Expo.*, 2013, pp. 3258–3265.

[76] O. C. Onar, S. Campbell, P. Ning, J. M. Miller, and Z. Liang, "Fabrication and evaluation of a high performance SiC inverter for wireless power transfer applications," in *Proc. IEEE Workshop Wide Bandgap Power Devices Appl.*, 2013, pp. 125–130.

[77] M. Scudiere and J. McKeever, "Wireless power transfer for electric vehicles," *SAE Int.*, Warrendale, PA, USA, SAE Technical Paper 2011-01-0354, Apr. 2011.

[78] O. C. Onar, J. M. Miller, S. L. Campbell, C. Coomer, C. P. White, and L. E. Seiber, "Oak ridge national laboratory wireless power transfer development for sustainable campus initiative," in *Proc. IEEE Transp. Electrification Conf. Expo.*, 2013, pp. 1–8.

[79] M. Budhia, G. A. Covic, J. T. Boys, and C.-Y. Huang, "Development and evaluation of single sided flux couplers for contactless electric vehicle charging," in *Proc. IEEE Energy Convers. Congr. Expo.*, 2011, pp. 614–621.

[80] S. Y. Choi, B. W. Gu, Y. S. Jeong, and C. T. Rim, "The history of wireless power transfer systems for roadway powered electric vehicles," *IEEE J. Emerg. Sel. Topics Power Electron.*, vol. 3, no. 1, pp. 18–36, Mar. 2015.

[81] S. Lee, J. Huh, C. Park, N.-S. Choi, G.-H. Cho, and C.-T. Rim, "On-line electric vehicle using inductive power transfer system," in *Proc. IEEE Energy Convers. Congr. Expo.*, 2010, pp. 1598–1601.

[82] J. Huh, S. Lee, C. Park, G.-H. Cho, and C.-T. Rim, "High performance inductive power transfer system with narrow rail width for on-line electric vehicles," in *Proc. IEEE Energy Convers. Congr. Expo.*, 2010, pp. 647–651.

[83] B. Song, J. Shin, S. Lee, S. Shin, Y. Kim, S. Jeon, and G. Jung, "Design of a high power transfer pickup for on-line electric vehicle (OLEV)," in *Proc. IEEE Int. Electric Vehicle Conf.*, 2012, pp. 1–4.

[84] C.-S. Wang, O. H. Stielau, and G. Covic, "Design considerations for a contactless electric vehicle battery charger," *IEEE Trans. Ind. Electron.*, vol. 52, no. 5, pp. 1308–1314, Oct. 2005.

[85] C.-S. Wang, G. Covic, and O. H. Stielau, "Power transfer capability and bifurcation phenomena of loosely coupled inductive power transfer systems," *IEEE Trans. Ind. Electron.*, vol. 51, no. 1, pp. 148–157, Feb. 2004.

[86] E. Culurciello and A. Andreou, "Capacitive inter-chip data and power transfer for 3-D VLSI," *IEEE Trans. Circuits Syst. II Exp. Briefs*, vol. 53, no. 12, pp. 1348–1352, Dec. 2006.

[87] A. Sodagar and P. Amiri, "Capacitive coupling for power and data telemetry to implantable biomedical microsystems," in *Proc. IEEE 4th Int. Conf. Neural Eng.*, 2009, pp. 411–414.

[88] J. Dai and D. C. Ludois, "Biologically inspired coupling pixilation for position independence in capacitive power transfer surfaces," in *Proc. IEEE 30th Annu. Appl. Power Electron. Conf. Expo.*, 2015, to be published.

[89] C. Liu, A. Hu, G. Covic, and N. C. Nair, "Comparative study of CCPT systems with two different inductor tuning positions," *IEEE Trans. Power Electron.*, vol. 27, no. 1, pp. 294–306, Jan. 2012.

[90] C. Liu, A. Hu, B. Wang, and N. C. Nair, "A capacitively coupled contactless matrix charging platform with soft switched transformer control," *IEEE Trans. Ind. Electron.*, vol. 60, no. 1, pp. 249–260, Jan. 2013.

[91] L. Chao, A. P. Hu, and D. Xin, "A contactless power transfer system with capacitively coupled matrix pad," in *Proc. IEEE Energy Convers. Congr. Expo.*, 2011, pp. 3488–3494.
[92] L. Chao and A. P. Hu, "Steady state analysis of a capacitively coupled contactless power transfer system," in *Proc. IEEE Energy Convers. Congr. Expo.*, 2009, pp. 3233–3238.
[93] M. Kline, I. Izyumin, B. Boser, and S. Sanders, "Capacitive power transfer for contactless charging," in *Proc. IEEE 26th Annu. Appl. Power Electron. Conf. Expo.*, 2011, pp. 1398–1404.
[94] 2011." Murata taps capacitive-coupled method for wireless power transfer," [Online]. Available: http://www.murata.com/products/article/pdf/ta1191.pdf
[95] D. C. Ludois, J. K. Reed, and K. Hanson, "Capacitive power transfer for rotor field current in synchronous machines," *IEEE Trans. Power Electron.*, vol. 27, no. 11, pp. 4638–4645, Nov. 2012.
[96] D. C. Ludois, K. Hanson, and J. K. Reed, "Capacitive power transfer for slip ring replacement in wound field synchronous machines," in *Proc. IEEE Energy Convers. Congr. Expo.*, 2011, pp. 1664–1669.
[97] C. Liu, A. P. Hu, and N. K. C. Nair, "Modelling and analysis of a capacitively coupled contactless power transfer system," *Power Electron. IET*, vol. 4, pp. 808–815, 2011.
[98] H. Funato, H. Kobayashi, and T. Kitabayashi, "Analysis of transfer power of capacitive power transfer system," in *Proc. IEEE 10th Int. Conf. Power Electron. Drive Syst.*, 2013, pp. 1015–1020.
[99] H. Kobayashi, H. Funato, and Y. Chiku, "Enhancement of transfer power of capacitive power transfer system using cascaded one pulse switching active capacitor (C-OPSAC) with three-level operation," in *Proc. 7th Power Electron. Motion Control Conf.*, 2012, vol. 2, pp. 884–888.
[100] M. P. Theodoridis, "Effective capacitive power transfer," *IEEE Trans. Power Electron.*, vol. 27, no. 12, pp. 4906–4913, Dec. 2012.
[101] J. Dai and D. C. Ludois, "Wireless electric vehicle charging via capacitive power transfer through a conformal bumper," in *Proc. IEEE 30th Annu. Appl. Power Electron. Conf. Expo.*, 2015, to be published.

Jiejian Dai (S'13) received the B.S. degree in electrical engineering from Zhejiang University, Hangzhou, China. He is currently working toward the Ph.D. degree in electrical engineering at the University of Wisconsin, Madison, WI, USA, with the Wisconsin Electric Machines and Power Electronics Consortium.

His research interests include power electronic circuit design and control.

Daniel C. Ludois (S'08–M'12) received the B.S. degree in physics from Bradley University, Peoria, IL, USA, in 2006, and the M.S. and Ph.D. degrees in electrical engineering from the University of Wisconsin (UW-Madison), Madison, WI, USA, in 2008, and 2011, respectively.

He returned to UW-Madison in the fall of 2013 as a Faculty Member with the Department of Electrical and Computer Engineering and the Wisconsin Electric Machines and Power Electronics Consortium. His research interests include power electronics, electric machines, applied electromagnetics, and engineering design for sustainability.

Dr. Ludois received the USA National Science Foundation CAREER Award in 2015 for his work on electrostatic machines. He is also a CTO at C-Motive Technologies, a company he cofounded in 2011 to develop advanced electric motor/generator technologies utilizing capacitive coupling techniques.